Improved Simulation of Clear-Sky Shortwave Radiative Transfer in the CCC-GCM

HOWARD W. BARKER*

Cloud Physics Research Division (ARMP), Atmospheric Environment Service, Downsview, Ontario, Canada

ZHANQING LI

Applications Division, Canada Centre for Remote Sensing, Ottawa, Ontario, Canada

(Manuscript received 2 August 1994, in final form 6 February 1995)

ABSTRACT

The disposition of mean July clear-sky solar radiation in the Canadian Climate Centre second-generation general circulation model (CCC-GCMII) was analyzed by comparing top of the atmosphere (TOA) net fluxes with earth radiation budget experiment (ERBE) data and atmospheric and surface net fluxes with values inferred from Li's algorithm using ERBE data and European Centre for Medium-Range Weather Forecasts precipitable water data. GCMII tended to reflect ~ 5 W m^{-2} too much to space. Corresponding atmospheric and surface absorption, however, tended to be too low and high, respectively, by ~ 30 W m^{-2} over much of the Northern Hemisphere. These results were echoed when GCMII atmospheric absorption was compared to estimated results from Li's algorithm driven by GCMII TOA albedo and precipitable water.

The latest version of the CCC-GCM (GCMIII) has numerous upgrades to its clear-sky solar radiative transfer algorithm, the most important of which involve water vapor transmittances and aerosols that tend to enhance atmospheric absorptance. GCMIII's water vapor transmittance functions derive from Geophysical Fluid Dynamics Laboratory line-by-line results, whereas GCMII's were based on Air Force Geophysical Laboratory data. GCMIII includes crude distributions of background tropospheric aerosols, whereas GCMII neglected aerosols.

Li's algorithm was then driven by GCMIII data, and atmospheric absorption of solar radiation by GCMIII was assessed. Differences between GCMIII's and Li's atmospheric absorption over land were almost always within 5 W m^{-2}. Over oceans, differences were mostly between -5 W m^{-2} and -15 W m^{-2}. This apparent underestimation over GCMIII's oceans probably stems from the algorithm's use of a thin, highly absorbing aerosol.

1. Introduction

Earth's climate is determined mostly by the disposition of solar radiation within the system. It is, therefore, imperative that GCMs, especially those with interactive oceans and sea ice, model properly solar radiative transfer. This, however, is a difficult task for it requires GCMs to 1) portray proper spatial and temporal distributions of clouds, aerosols, and gases and parameterize accurately their radiative properties (Slingo and Slingo 1991; Ramaswamy and Freidenreich 1992; Kiehl and Briegleb 1993); 2) take into account cloud variability over vast ranges of scales (Barker and Davies 1992; Cahalan et al. 1994); and 3) account for variable surface albedos (Li and Garand 1994). Assessing whether GCMs fulfill these requirements is hampered by a paucity of reliable and suitable observations. Thanks to advances in remote sensing techniques, however, it is becoming possible to compare the disposition of solar fluxes in GCMs to values inferred from satellite data (Li and Barker 1995).

Estimation of downwelling solar irradiance at the surface using satellite data has been taking place for some time (Gauthier et al. 1980; Pinker and Ewing 1985) and inference of the complete solar budget has begun (e.g., Cess and Vulis 1989; Li et al. 1993a). Since a comparison of solar fluxes at the top of the atmosphere (TOA) between the Canadian Climate Centre second-generation general circulation model (CCC-CGMII) (McFarlane et al. 1992) and Earth Radiation Budget Experiment (ERBE) data has been reported (Barker et al. 1994), this paper focuses on the ability of two versions of the CCC-GCM to partition absorbed solar radiation between the surface and atmosphere for clear-sky conditions. Analyses were restricted to clear skies because some cloud optical properties are still being adjusted in the latest version of the GCM, and also because inference of surface net solar fluxes from space appears to be hampered by substantially nonplanar clouds (Li et al. 1995b).

---

* Additional affiliation: Department of Geography, McMaster University, Hamilton, Ontario, Canada.

Corresponding author address: Dr. Howard W. Barker, Cloud Physics Research Division (ARMP), Atmospheric Environment Service, 4905 Dufferin Street, Downsview, ON M3H 5T4, Canada.
E-mail: barker@armph4.dow.on.doe.ca

Barker et al. (1994) identified several shortwave radiative characteristics of the CCC-GCMII that needed improvement. Many of these were crucial for clear skies; for example, a deficit of precipitable water and ocean and snow albedo. In addition, this paper shows the need to include at least background tropospheric aerosols and to improve water vapor transmittances. Due to these shortcomings in GCMII, its surface and atmosphere absorb alarmingly large and small amounts of solar radiation, respectively. Moreover, this problem is encountered by many GCMs (Li and Barker 1995).

Section 2 of this paper compares clear-sky solar fluxes absorbed by GCMII's surface and atmosphere with corresponding values inferred from ERBE data (Li and Leighton 1993) by the algorithm of Li et al. (1993a) (heretoafter referred to as Li's algorithm). Then, Li's algorithm was driven by GCMII data, which isolated differences due to radiation codes only. In section 3, modifications to GCMII's clear-sky solar radiation characteristics are described (CCC-GCMIII). In section 4, clear-sky solar fluxes obtained with the new CCC-GCMIII are compared to values from Li's algorithm. Concluding remarks are made in section 5.

2. Disposition of clear-sky solar radiation in GCMII

McFarlane et al. (1992) and Barker et al. (1994) have documented and analyzed the radiative characteristics of the CCC-GCMII. GCMII data used in this section were from its original Atmospheric Model Intercomparison Project (AMIP) simulation (Gates 1992). Only mean values for four Julys were presented (1985–88) and they were compared to corresponding fluxes from ERBE datasets. The essence of these results were almost identical to those for four Januarys.

Li et al. (1993a) devised an algorithm (see the appendix) for inferring net shortwave radiation at the surface (and in the atmosphere) that uses local planetary albedo, precipitable water, and cosine of the solar zenith angle. An empirical study (Li et al. 1993b) using collocated satellite and land surface tower measurements suggested that clear-sky surface flux estimates have very small mean-bias errors and only moderate random errors. Li's algorithm was applied to monthly mean ERBE and European Centre for Medium-Range Weather Forecasts (ECMWF) precipitable water datasets to generate a 5-yr climatology of surface and atmosphere absorbed solar fluxes (Li and Leighton 1993). This dataset is referred to as ERBE/SRB (surface radiation budget). Only the clear-sky subset of the ERBE/SRB dataset was employed in this study. Thus, clear-sky ERBE/SRB and application of Li's algorithm to GCMII clear-sky TOA data defined the standard to which the GCM's fluxes were compared.

Figure 1 shows the difference in disposition of clear-sky solar radiation between GCMII and ERBE data for July in which the atmospheric and surface components are from ERBE/SRB. Many differences at the TOA can be attributed to surface albedo differences as discussed in detail by Barker et al. (1994). For example, GCMII's northern ice margin is much too bright, many of its Northern Hemisphere deserts are too dark (especially the Sahara), and its northern boreal forests are too reflective due to exclusion of relatively dark freshwater lakes (the opposite is true during winter when lakes are snow covered). For the most part, GCMII's TOA reflectance over oceans is too low (i.e., net solar at the TOA is too large). This is due to improper surface albedo specification and lack of maritime aerosols and will be discussed in section 3.

While some of the extreme differences in TOA flux are evident in the difference of net surface flux (e.g., northern pack-ice margin), GCMII's surface tends to absorb substantially more solar radiation than ERBE/SRB values. In fact, over the Northern Hemisphere, GCMII ocean surfaces systematically absorb 30 W m^{-2} too much. For this to be due exclusively to underestimated ocean albedo, it would have to be more than 0.15 too low. This is not the case as the albedo for tropical and midlatitude summer oceans is about 0.06 (Cox and Munk 1956; Payne 1972), while the corresponding value in GCMII is about 0.08 (Barker et al. 1994). This means that the excess absorption is due to excessive irradiance. While GCMII does neglect aerosols, typical maritime aerosols almost certainly do not attenuate surface irradiance by 35 W m^{-2}.

As expected, the difference between GCMII and ERBE/SRB atmospheric absorption shows that much of the overestimated flux at the surface stems from an equally severe underestimation of atmospheric absorption. Over the Northern Hemisphere, the underestimation is generally between 20 and 40 W m^{-2}. Since there is little distinction between land and ocean, this bias is independent of surface albedo. Li's algorithm is known to yield excessive atmospheric absorptances for very low values of precipitable water, especially for long direct-beam slant paths. At most, however, the error is $\sim$10 W m^{-2}, and so only partly explains the large discrepancies (which exceed 35 W m^{-2}) poleward of 60°N as shown in Fig. 1. Furthermore, Li's algorithm uses a highly absorptive, albeit thin, Arctic aerosol, and this leads to excessive atmospheric absorption especially over remote oceans. Hence, the magnitude of some absorption differences shown in Fig. 1 are probably too large by about 5–10 W m^{-2}. Otherwise, much confidence has to be placed in Li's clear-sky algorithm following its excellent agreement with surface data for land sites (mean-bias error less than 1 W m^{-2}) (see Li et al. 1993b; Li et al. 1995a). The fact that GCMII appears to underestimate precipitable water by $\sim$15% (Barker et al. 1994) accounts for at most about 5 W m^{-2}. Thus, the only remaining conventional hypotheses capable of addressing systematic anomalies rivaling those in Fig. 1 are neglect of aerosols and faulty broadband transmittance parameterizations of atmospheric gases.

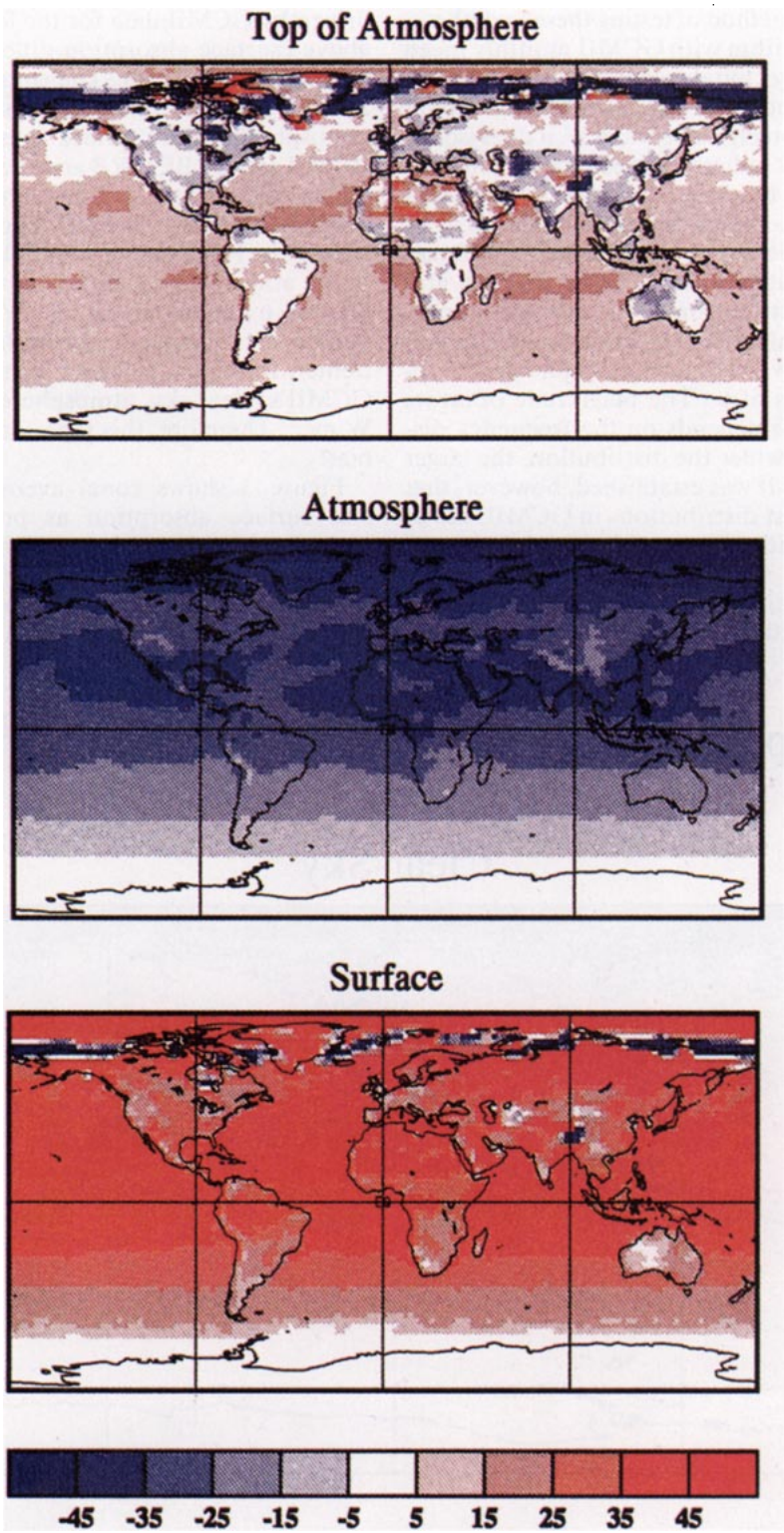

FIG. 1. Difference (in W m^{-2}) for net clear-sky solar fluxes at the TOA, in the atmosphere, and at the surface between GCMII and ERBE data. ERBE values for surface and atmospheric absorption were obtained by applying Li's algorithm to ERBE TOA albedo and ECMWF precipitable water.

The most direct method of testing these hypotheses is to drive Li's algorithm with GCMII monthly mean TOA albedo and precipitable water vapor amounts. While this does not provide information about GCMII's deficit of precipitable water w, it does isolate differences between radiative transfer algorithms. It should be noted, however, that all of GCMII's monthly mean fluxes were integrated, whereas Li's algorithm was applied to monthly mean TOA fluxes and precipitable water vapor $\bar{w}$. Since for each grid point there is a distribution of w, this will impact Li's estimates: the algorithm is a nonlinear function of w and tends to overestimate atmospheric absorption at small values of w. The magnitude of errors due to use of just $\bar{w}$ depends on the frequency distribution of w: the wider the distribution, the larger the overestimation. It was established, however, that even for the broadest distributions in GCMII, use of just $\bar{w}$ in the algorithm overestimates atmospheric absorption by only ~ 2 W m^{-2}.

Figure 2 shows differences between atmospheric absorption predicted by GCMII and Li's algorithm driven by GCMII data for the four Julys considered above (surface absorption differences are the same but of opposite sign). The similarity between Figs. 2 and 1 illustrates that most of the discrepancy in atmospheric and surface absorptances between GCMII and ERBE/SRB arise because of algorithmic differences (which includes aerosols), not GCMII's precipitable water deficit. Thus, for most of the Northern Hemisphere, GCMII under(over)-estimates atmospheric (surface) absorption of solar radiation by more about 25 W m^{-2} (same in the Southern Hemisphere during January). This is extremely important since for the summer hemisphere, GCMII's clear-sky atmosphere absorbs about 80 W m^{-2}. Therefore, this represents more than a 30% bias!

Figure 3 shows zonal averages of atmospheric and surface absorption as predicted by GCMII and Li's algorithm driven by both ERBE/ECMWF and GCMII data. Here the systematic biases are striking. Also, from this plot it might appear that Li's algorithm is fairly insensitive to input

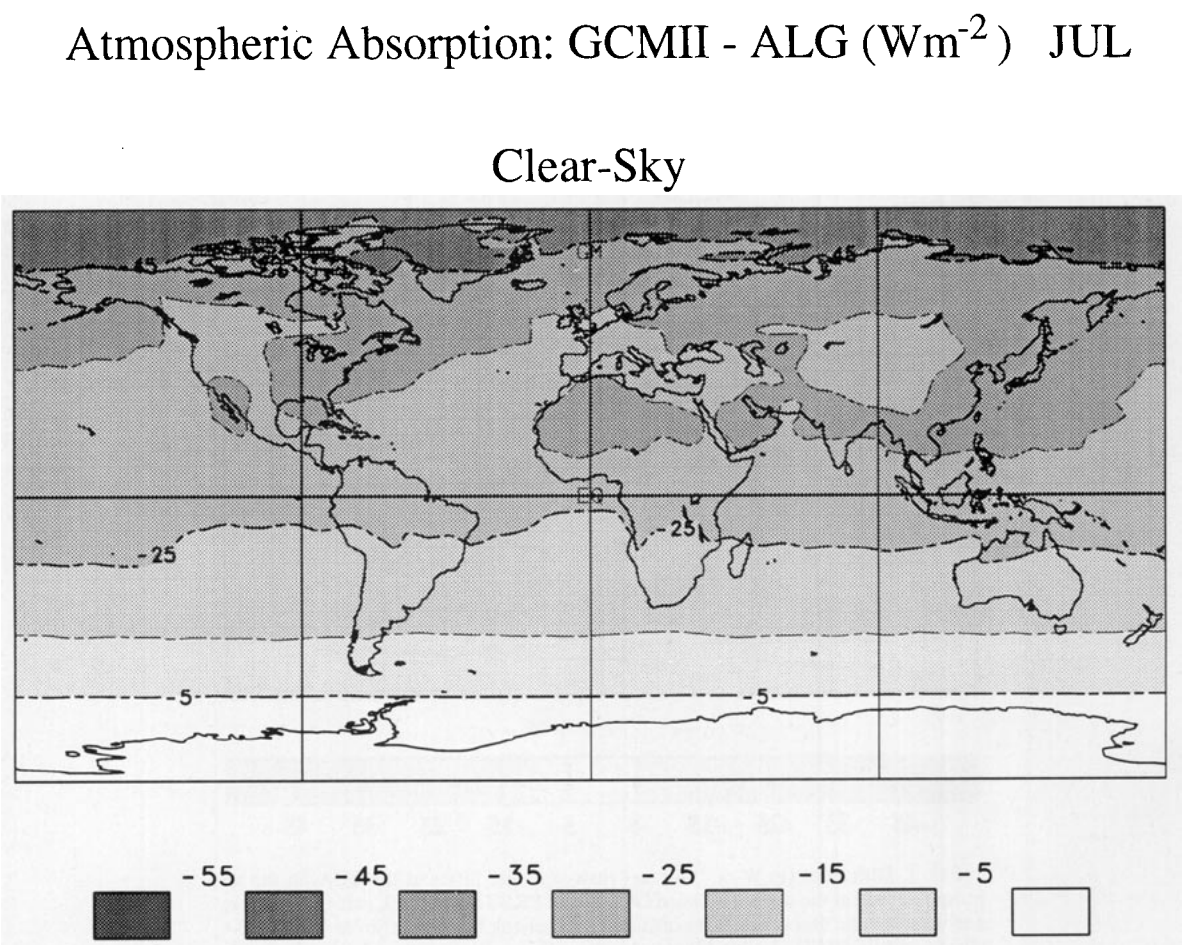

FIG. 2. Difference (in W m^{-2}) for clear-sky atmospheric solar absorption between GCMII and Li's algorithm driven by GCMII TOA albedo and precipitable water. Contour interval is 10 W m^{-2}.

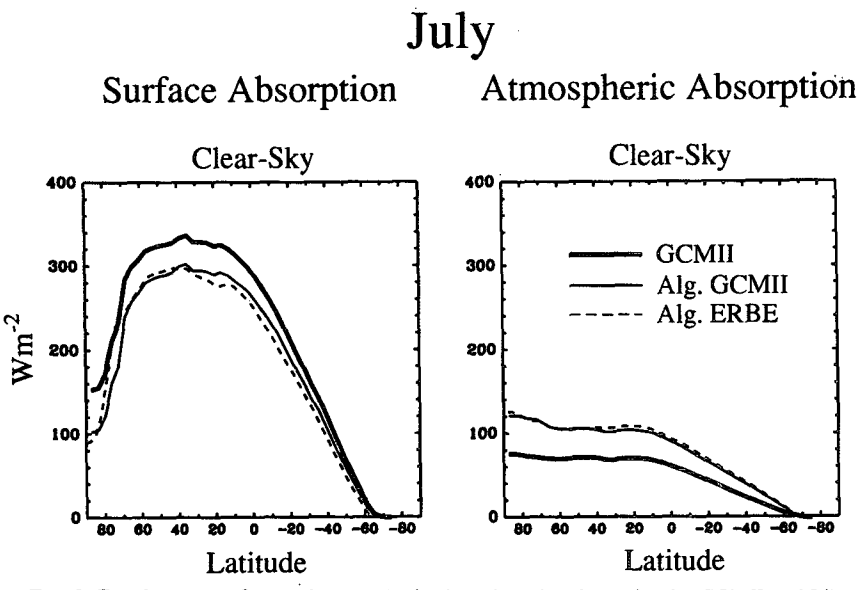

FIG. 3. Zonal mean surface and atmospheric clear-sky solar absorption by GCMII and Li's algorithm using ERBE and ECMWF data and GCMII data.

conditions. This, however, is not the case: Fig. 1 shows that, in general, GCMII reflects too little, and when this is used in Li's algorithm it predicts more atmospheric and surface absorption relative to when ERBE fluxes are used. However, the fact that GCMII's atmosphere is too dry forces the algorithm to predict less atmospheric and more surface absorption relative to ERBE/SRB. Thus, the two compensating factors affecting Li's estimates of atmospheric absorption when driven by GCMII data tend to cancel out, making those estimates approximately equal to the ERBE/SRB estimates. For the surface, however, both factors lead to overestimation of surface absorption relative to ERBE/SRB, which is clearly the case except for the northern pack ice margin and ~50°N (boreal forests) where excessive GCMII reflectances force Li's estimates of surface absorption down relative to ERBE/SRB.

One should be aware that in order for GCMII and Li's algorithm forced by GCMII data to agree on clear-sky atmospheric a_a and surface a_s absorptance, GCMII is not necessarily required to increase its globally averaged atmospheric absorption by about 25 W m^{-2}. This is because changes to GCMII's radiative transfer code and atmosphere lead to changes in Li's estimates of a_s and a_a. Differentiating (A1) in the appendix leads to changes to Li's estimates of a_s and a_a defined by

$$\Delta a_s = -\beta(\overline{\mu_0}, \bar{w})(\Delta\alpha_p + \Delta\alpha_p^{\Delta\bar{w}} + \Delta\alpha_p^{\Delta\text{trans}} + \Delta\alpha_p^{\Delta\tau}) + \frac{\partial a_s}{\partial \bar{w}}\Delta\bar{w}, \quad (1a)$$

and

$$\Delta a_a = -[1 - \beta(\overline{\mu_0}, \bar{w})](\Delta\alpha_p + \Delta\alpha_p^{\Delta\bar{w}} + \Delta\alpha_p^{\Delta\text{trans}} + \Delta\alpha_p^{\Delta\tau}) - \frac{\partial a_s}{\partial \bar{w}}\Delta\bar{w}, \quad (1b)$$

where $\beta(\overline{\mu_0}, \bar{w})$ is from Li's algorithm (see the appendix) in which $\overline{\mu_0}$ is monthly mean cosine of the solar zenith angle, and $\Delta\alpha_p^{\Delta\bar{w}}$, $\Delta\alpha_p^{\Delta\text{trans}}$, and $\Delta\alpha_p^{\Delta\tau}$ represent changes to GCMII's TOA albedo α_p due to changes in $\bar{w}$, water vapor transmittance function, and aerosol optical depth τ, respectively. Other changes to α_p are encompassed in $\Delta\alpha_p$ and these might be caused by changing surface albedo, radiative transfer algorithm, and other gaseous transmittance functions. The second term on the rhs of (1a) and (1b) represents changes to Li's surface absorption due to changes in $\bar{w}$ and can be shown to be (see the appendix)

$$\frac{\partial a_s}{\partial \bar{w}}\Delta\bar{w} = -0.0108\bar{w}^{-1/2}\left[1 + \frac{3.162}{\overline{\mu_0}}(1 - e^{-\overline{\mu_0}})\right]. \quad (2)$$

Thus, for example, if $\bar{w}$ increased by 15% in GCMII, Li's algorithm would predict approximately an additional 4 W m^{-2} absorbed by the atmosphere on a globally averaged basis. If, on the other hand, GCMII absorptances are to match ERBE/SRB data, GCMII's atmosphere must absorb approximately an additional 25 W m^{-2}.

3. Improvements to clear-sky solar radiation: GCMIII

Several deficiencies in GCMII related to radiation were identified both by Barker et al. (1994) and in the

previous section of this paper. The purpose of this section is to explain briefly changes to the clear-sky solar radiative transfer characteristics of GCMII (the new version will be referred to as GCMIII). While several changes involving clouds and longwave radiative transfer have either been done or are in progress, they are not reported here.

a. Earth's orbital parameters

In all versions of the CCC-GCM up until GCMIII, it was assumed that Earth revolved around the Sun in a circular orbit with a solar constant of 1370 W m^{-2}. This has been corrected following Berger and Loutre (1993). Also, the solar constant used in AMIP and in GCMIII is 1365 W m^{-2}.

b. Surface albedo

1) OCEAN ALBEDO

As discussed by Barker et al. (1994), the ocean albedo used in GCMII was a function of latitude only. This produced seasonal albedo changes that were out of phase as well as being of incorrect magnitude. The description of direct-beam ocean albedo used in GCMIII is essentially Hansen et al.'s (1983) parameterization of Cox and Munk's (1956) Fresnel, Gaussian ergodic wave theory:

$$\alpha_s = 0.036 + 0.0421x^2 + 0.128x^3 - 0.04x^4 + \left(\frac{3.12}{5.68 + v} + \frac{0.074x}{1.0 + 3.0v}\right)x^5, \quad (3)$$

where $x = 1 - \mu_0$ and v is wind speed in the lowest model layer. The leading term in (3) has been increased from 0.021 in order to match ERBE TOA clear-sky albedos. A small systematic increase to Cox and Munk's theoretical results could be justified, however, because they did not consider suspended sediment, plankton, and bubbles from breaking waves.

Figure 4 shows the fractional difference between the June–July–August (JJA) surface albedo defined in GCMIII and GCMII's 1 × (CO_2) simulation (McFarlane et al. 1992). The only notable difference over the oceans is poleward of 30°N where there was a systematic reduction of between 10% and 30% or about 0.015 in absolute albedo terms.

2) LAND ALBEDO

Figure 4 shows that several minor modifications to land surface albedo (D. Verseghy 1994, personal communication) had little impact. In fact, many of the differences shown in Fig. 4 arise from differences in soil moisture. For example, albedo reductions across southern Sahara and the Saudi peninsula stem from excessive precipitation. In actuality, the dry, or basal, albedo for much of these regions was increased from ~0.35 in GCMII to ~0.45 in accordance with satellite-inferred values (Barker and Davies 1989a; Li and Garand 1994). This illustrates the difficulty in assigning surface albedo in some regions: albedo depends on soil moisture and soil moisture in turn depends on albedo.

c. Aerosol–air two-stream approximation and optical properties

For computation of solar fluxes for mixtures of aerosols and air molecules, GCMII uses a two-term series expansion of Coakley and Chýlek's (1975) two-stream approximation, in which the direct beam was represented implicitly (Barker and Davies 1989a). Also, it was assumed that the direct and diffuse backscatter functions were defined as $(1 - g)/2$, where g is the effective asymmetry parameter of the air–aerosol mixture.

For GCMIII, Coakley and Chýlek's (1975) full (not truncated) two-stream approximation is used, as well as the proper backscatter functions, assuming the Henyey–Greenstein (1941) phase function. For upwelling radiation, the generalized diffuse backscatter function is used in which the upwelling beam is assumed to be a linear function of cosine of zenith angle (Barker 1994). For downwelling radiation, the direct-beam backscatter function $\beta(\mu_0)$ is used (Wiscombe and Grams 1976) and evaluated for the effective value of μ_0 (McFarlane et al. 1992). Due to its intractable nature, $\beta(\mu_0)$ was parameterized (Barker 1994) for the Henyey–Greenstein phase function as

$$\beta(\mu_0, g) = \frac{16.156e^{-7.439g} + \mu_0[-0.148 + g(0.731 - 0.639g)]}{32.312e^{-7.439g} + \mu_0(4.347e^{-3.248g} + \mu_0)}. \quad (4)$$

Equation (4) is accurate to 0.1% for g between 0.3 and 0.8 and all μ_0.

No aerosols were included in GCMII. Barker and Davies (1989b) used surface pyranometer and satellite data to demonstrate that GCMII's solar code required background tropospheric aerosols (neglecting aerosols, it overestimated surface irradiances by about 40 W m^{-2} at sites in Australia and Canada). In GCMIII, however, crude static distributions of background tropospheric aerosols are specified. The aerosols are assumed to be well mixed within the GCM's boundary layer, which rarely extends above about 800 mb (M. Lazare 1994,

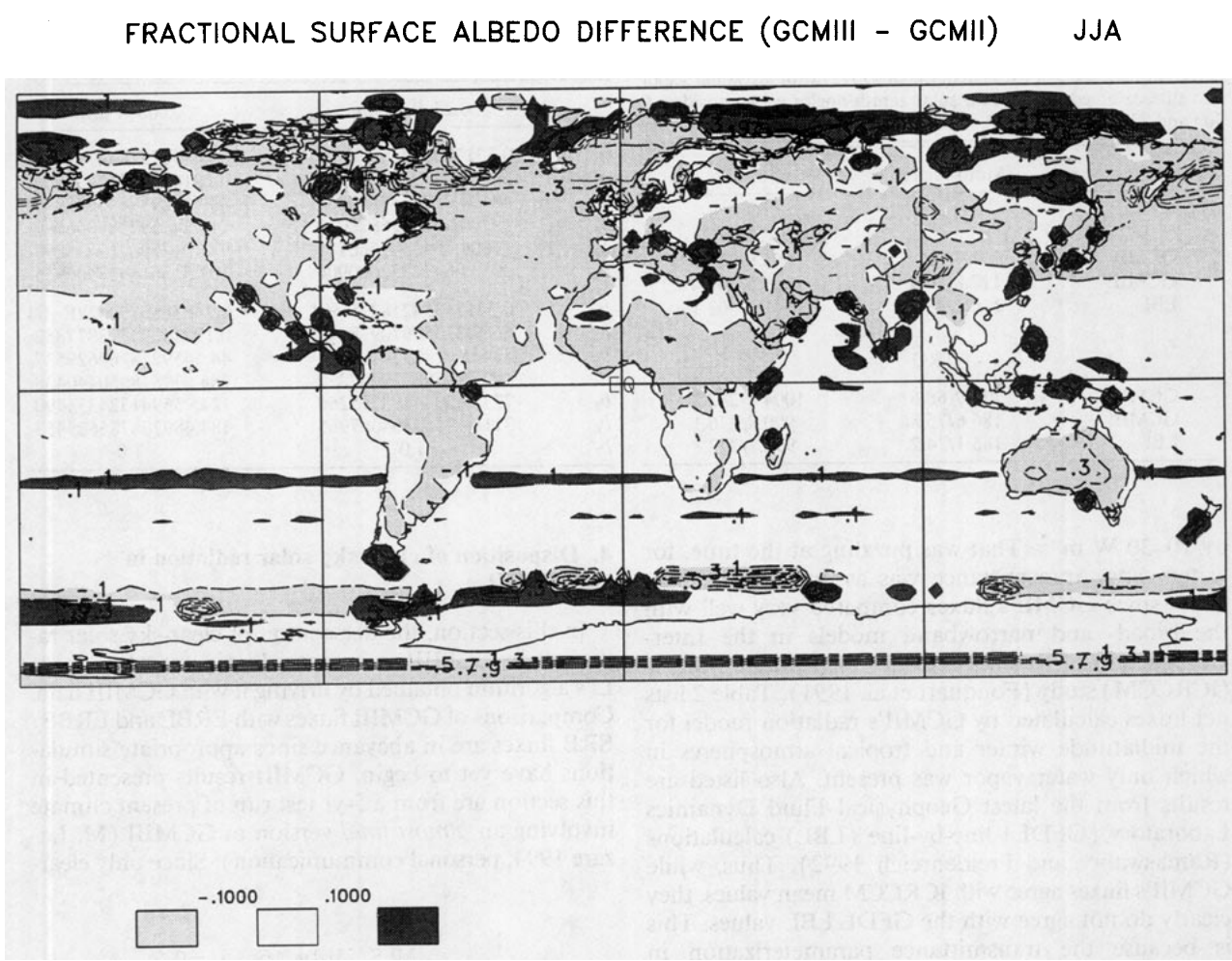

FIG. 4. Fractional difference in surface albedo α_s between GCMII and GCMIII: $[\alpha_s(\text{GCMIII}) - \alpha_s(\text{GCMII})]/\alpha_s(\text{GCMII})$ is plotted. Contour interval is 0.2.

personal communication). The optical properties depend on whether the aerosol is over land or ocean and are listed in Table 1. These values were obtained by weighting data listed by Tanre et al. (1984) with an extraterrestrial solar spectrum (Thekaekara 1974) and integrating across appropriate wavebands. Vertically integrated optical depths at a wavelength of 0.55 μm depend on latitude θ (rds) as

$$\tau = \begin{cases} 0.25 - 0.2\left(\frac{2}{\pi}\right)\text{abs}(\theta) & \text{over land} \\ 0.13 - 0.1\left(\frac{2}{\pi}\right)\text{abs}(\theta) & \text{over ocean,} \end{cases} \quad (5)$$

which is similar to that used by Coakley and Cess (1985). The global mean τ is, therefore, 0.12, which is close to the current best estimate of 0.105 (Jonas et al. 1995). Ultimately, aerosols will be prognostic variables with interactive sources, sinks, and optical properties.

d. Water vapor transmittance

When Barker and Davies (1989b) accounted for reasonable aerosol optical depths in GCMII's solar code, it still overestimated measured surface irradiances

TABLE 1. Single scattering albedo ω_0, asymmetry parameter g, and prefactor ξ used to extrapolate optical depth at 0.55 μm to entire spectral interval for aerosols used in GCMIII.

	ω_0	g	ξ
	0.25–0.68 μm		
Land	0.894	0.641	1.120
Ocean	0.988	0.745	1.020
	0.68–4 μm		
Land	0.801	0.651	0.448
Ocean	0.975	0.764	0.877

TABLE 2. Diurnal-mean atmospheric and surface solar absorption for GCMII, GCMIII, and LBL calculations (Ramaswamy and Freidenreich 1992) for the midlatitude winter (MLW) and tropical (TRO) atmospheres of McClatchey et al. (1972) with just water vapor and surface albedo of 0. Two solar zenith angles were considered: 30° and 75° (30° value/75° value). Units in watts per square meter.

	Atmosphere	Surface
	MLW	
GCMII	111.9/46.9	1065.6/305.0
GCMIII	117.8/50.4	1059.5/301.4
LBL	116.2/48.9	1061.6/303.1
	TRO	
GCMII	172.9/68.6	1004.7/283.3
GCMIII	186.6/75.8	990.8/276.1
LBL	185.1/74.2	992.7/277.8

TABLE 3. Coefficients for the two spectral interval water vapor transmittance parameterizations. Coefficients are for the Padé approximants in (6).

	0.25–0.68 μm	0.68–4 μm
a_1	0.3317135643657E−01	0.2483072744470E−04
a_2	666.431509309246735	0.19160832757432552
a_3	48424.0238037360250	43.2532957143248993
a_4	192701.219426828029	710.241597307866186
a_5	77004.7340385666175	973.017590222333297
a_6	3033.06472352620904	107.515616933906955
b_1	0.3317135421822E−01	0.2483886109422E−04
b_2	666.432550670978117	0.19244025713877852
b_3	48425.9782574785131	44.5459218767629537
b_4	192810.508779007272	784.679818650440438
b_5	77339.2094893395260	1245.55941324355490
b_6	3118.19655304067965	184.489708785625453
b_7	1.0	1.0

by 10–30 W m^{-2}. That was puzzling at the time, for water vapor transmittance was assumed to be adequate since GCMII's fluxes compared very well with the broad- and narrowband models in the Inter-Comparison of Radiation Codes for Climate Models (ICRCCM) study (Fouquart et al. 1991). Table 2 lists net fluxes calculated by GCMII's radiation model for the midlatitude winter and tropical atmospheres in which only water vapor was present. Also listed are results from the latest Geophysical Fluid Dynamics Laboratory (GFDL) line-by-line (LBL) calculations (Ramaswamy and Freidenreich 1992). Thus, while GCMII's fluxes agree with ICRCCM mean values, they clearly do not agree with the GFDL LBL values. This is because the transmittance parameterization in GCMII derived from Air Force Geophysical Laboratory line absorption data (Rothman 1981).

A new set of broadband water vapor parameterizations were derived from the GFDL LBL data for use in GCMIII and the net fluxes are also listed in Table 2. GCMIII's estimates agree quite well with the GFDL values. The transmittance functions were parameterized as a function of effective photon pathlength u (g m^{-2}) using Padé approximants as

$$T = \frac{\sum_{n=1}^{6} a_n u^n}{\sum_{n=1}^{7} b_n u^n}, \qquad (6)$$

where the coefficients a_n and b_n are listed in Table 3. Figure 5 shows vertical distributions of solar heating rates for the midlatitude standard summer atmosphere as computed by the radiation codes used in GCMII and GCMIII. These are clear-sky, diurnal averages applicable to 15 July with surface albedo 0.2 and no aerosol. For much of the troposphere, GCMIII's heating rates exceed GCMII's by more than 10%.

4. Disposition of clear-sky solar radiation in GCMIII

In this section, the disposition of clear-sky solar radiation in GCMIII is compared only to values from Li's algorithm obtained by driving it with GCMIII data. Comparisons of GCMIII fluxes with ERBE and ERBE/SRB fluxes are in abeyance since appropriate simulations have yet to begin. GCMIII results presented in this section are from a 5-yr test run of present climate involving an *almost final* version of GCMIII (M. Lazare 1994, personal communication). Since only clear-

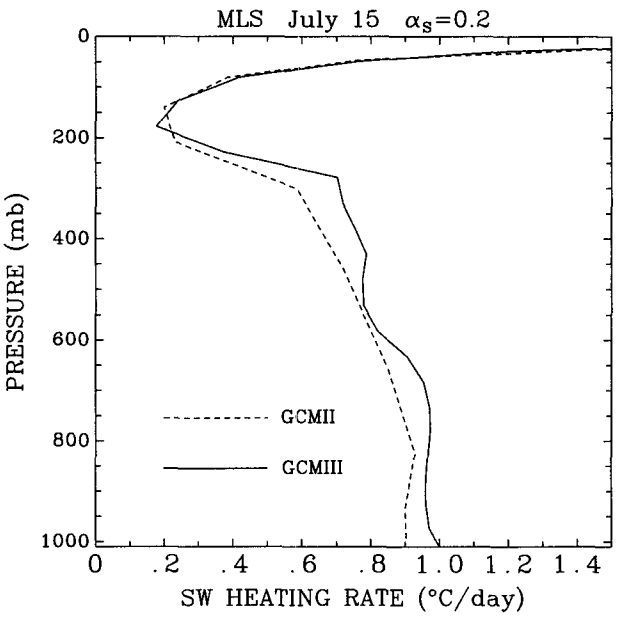

FIG. 5. Diurnal average, vertical distribution of shortwave heating rates predicted by GCMIII and GCMII for the cloudless, midlatitude summer standard atmosphere for 15 July at 45°N with surface albedo of 0.2.

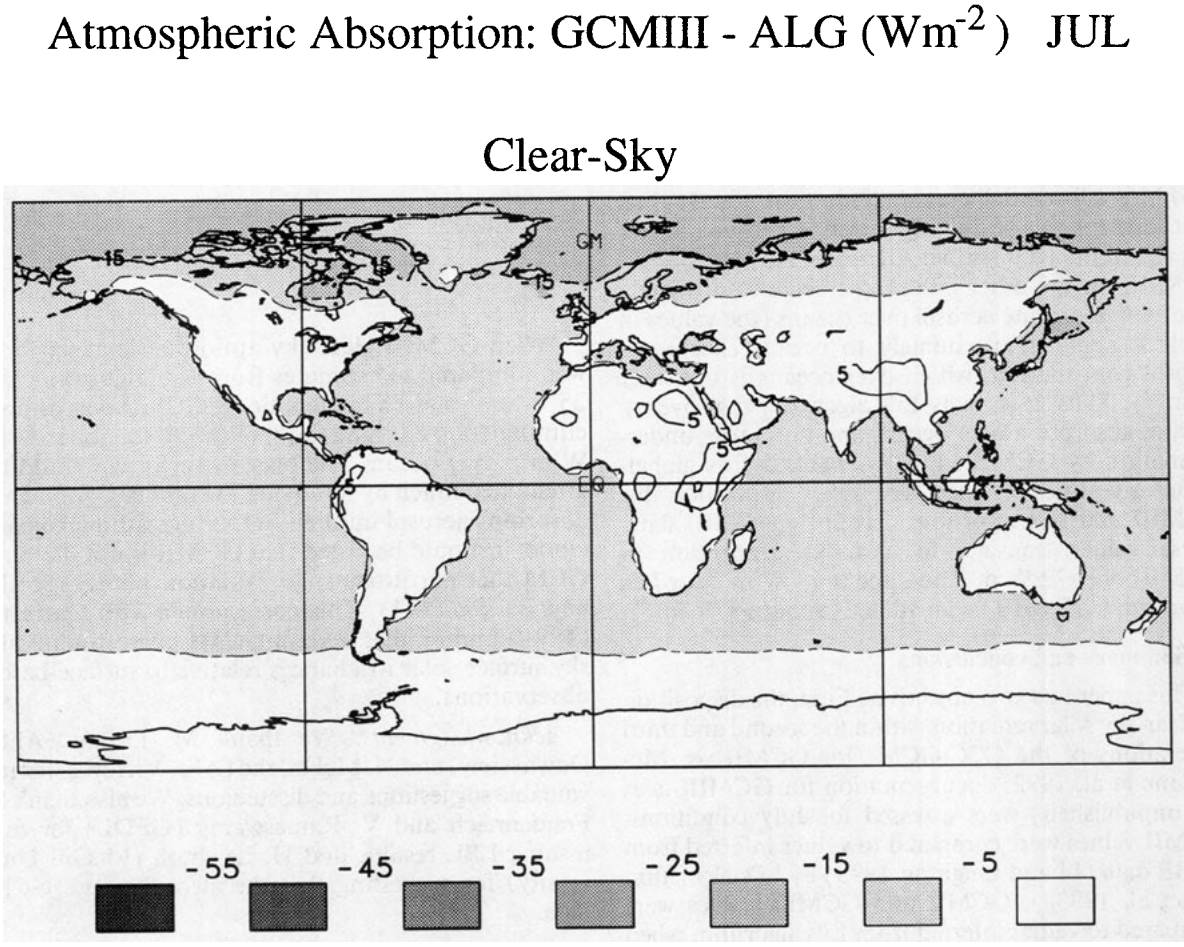

FIG. 6. As in Fig. 2 except for GCMIII.

sky solar fluxes are discussed, differences between results presented here and those in the final version of GCMIII will differ only slightly (due possibly to changes in the distribution of water vapor). Furthermore, results in this section apply to CO_2 of 330 ppmv. GCMIII is effectively a T48 resolution spectral model with 30 layers. It differs significantly from GCMII in many respects involving both numerics and representation of physical processes. Full documentation can be expected within the next few years.

Figure 6 shows the difference between clear-sky atmospheric absorption for GCMIII and Li's algorithm driven by GCMIII data. Relative to Figs. 1 and 2, the agreement seen in Fig. 6 is striking, especially over land where it is almost always within 5 W m^{-2}. The exception is poleward of ~60°N, where GCMIII absorbs too little by more than 5 W m^{-2}. This is probably because Li's algorithm overestimates absorption for small water vapor amounts.

Compared to the performance of GCMII, GCMIII has closed the gap between Li's estimates of atmospheric absorption for land points by about 25 W m^{-2}. Using the standard midlatitude summer atmosphere to represent mean global conditions, Table 4 lists the approximate contribution of several variables to enhanced absorption. Increasing the humidity adds about 4 W m^{-2}, while new water vapor transmittance functions contributed 5 W m^{-2}. Tropospheric aerosol increased absorption by almost 10 W m^{-2}, and reducing

TABLE 4. Approximate increases to GCMII's globally averaged atmospheric absorption over land due to improvements in several conditions, processes, and variables as discussed in the text. Results are for column model versions and represent diurnal-averages using the midlatitude summer atmosphere (McClatchey et al. 1972) with surface albedo of 0.2.

Condition/process/variable	Increased atmospheric absorption (W m^{-2})
Increased humidity	4
Water vapor transmittance	5
Tropospheric aerosol	10
Reduced TOA albedo	<3
Li's algorithm	3
	25

the GCM's TOA albedo allowed at most 3 W m^{-2} additional absorption. Roughly speaking, Li's algorithm is expected to overabsorb by around 3 W m^{-2}. These values sum to about approximately 25 W m^{-2}.

Over oceans, atmospheric absorption differences are -5 to -15 W m^{-2}. The primary reason for GCMIII absorbing substantially less radiation over ocean than over land relative to Li's algorithm is because, again, Li's algorithm assumes that Arctic aerosol covers earth. GCMIII, on the other hand, assumes a thin, weakly absorbing maritime aerosol over oceans (the values in Table 4 apply approximately to oceans except the aerosol contribution, which over oceans is only ~ 1 W m^{-2}). Thus, it is likely Li's algorithm that overestimates absorption over oceans and not a true underestimation by GCMIII. Finally, Table 5 lists global-mean quantities of clear-sky solar disposition for GCMIII and Li's algorithm driven by GCMIII data. These values translate to clear-sky absorption in GCMIII of ~ 72 W m^{-2} and about 78 W m^{-2} for Li's algorithm (GCMII's mean value is about 58 W m^{-2}).

5. Summary and conclusions

This paper had two objectives. First, the disposition of clear-sky solar radiation within the second and third generations of the CCC-GCM (for GCMII see McFarlane et al. 1992; documentation for GCMIII is as yet unpublished) were assessed for July conditions. GCMII values were compared to values inferred from ERBE data (Li and Leighton 1993) by Li's algorithm (Li et al. 1993a). GCMII and GCMIII values were compared to values inferred from Li's algorithm when it was driven by GCM data. The second objective was to document improvements to clear-sky solar radiative transfer in the CCC-GCM.

GCMII's TOA albedo is quite good though it underestimates systematically over oceans. Surface absorption by GCMII, however, is much greater than that inferred from ERBE data by Li's algorithm. This is countered by an equally severe underestimation of atmospheric absorption over most of the Northern Hemisphere (about -25 W m^{-2}). These trends were confirmed when GCMII values were compared to values from Li's algorithm when it was driven by GCMII data. In essence, GCMII's clear-sky atmosphere absorbs too little solar radiation.

The latest version of the CCC-GCM (GCMIII) has had several upgrades to its solar radiative transfer properties. The most important upgrades for clear-sky solar radiation involve new water vapor transmittance functions based on state-of-the-art LBL results (Ramaswamy and Freidenreich 1992); crude global distributions of background tropospheric aerosols; a new two-stream approximation for mixtures of air molecules and aerosols; and a solar zenith angle and wind speed dependent description of ocean surface albedo. Most of these updates tend to enhance atmospheric absorption relative to GCMII.

TABLE 5. Global-mean fractions of incoming solar radiation at the TOA that are reflected by the system, absorbed by the atmosphere, and absorbed by the surface for GCMIII and Li's algorithm driven with GCMIII data.

	GCMIII	Alg. (GCMIII)
Reflected	0.149	0.149
Atmosphere	0.209	0.229
Surface	0.642	0.622

When GCMIII clear-sky atmospheric absorption was compared to estimates from Li's algorithm, the 25 W m^{-2} bias characteristic of GCMII was almost eliminated over land and reduced to about -10 W m^{-2} over ocean. The biases over ocean could be attenuated much by removing the thin layer of highly absorbing aerosol implicit in Li's algorithm. To conclude, it should be noted that GCMII is not the only GCM that partitions solar radiation poorly (see Li and Barker 1994). This corresponds with Garratt's (1994) finding that several GCMs overestimate all-sky surface solar irradiances relative to surface-based observations.

Acknowledgments. We thank M. Lazare (AES-Downsview) and N. McFarlane (AES-Victoria) for invaluable suggestions and discussions. We also thank S. Freidenreich and V. Ramaswamy (GFDL) for furnishing LBL results, and H. Leighton (McGill University) for suggesting that the algorithm use GCM data.

APPENDIX

This appendix presents briefly Li et al.'s (1993a) clear-sky algorithm that was used throughout this study. This algorithm relates surface a_s and atmospheric a_a absorptances to planetary albedo α_p, precipitable water w, and cosine of the solar zenith angle μ_0:

$$a_s = \alpha(\mu_0, w) - \beta(\mu_0, w)\alpha_p,$$
$$a_a = 1 - a_s - \alpha_p, \tag{A1}$$

where

$$\alpha(\mu_0, w) = 1 - \frac{A}{\mu_0} - \frac{B}{(\mu_0)^{1/2}} + \frac{1}{\mu_0}(1 - e^{-\mu_0})[C - Dw^{1/2}],$$

and

$$\beta(\mu_0, w) = 1 + E + F\ln(\mu_0) + G + Hw^{1/2},$$

in which

$$A = -0.01124 \quad E = 0.0815$$
$$B = 0.1487 \quad F = 0.0139$$
$$C = 0.0699 \quad G = -0.0273$$
$$D = 0.0683 \quad H = 0.0216.$$

Fluxes are obtained by multiplying the absorptances in (A1) by the time-dependent incoming solar flux at the TOA.

REFERENCES

Barker, H. W., 1994: A parameterization and generalization of backscatter functions for two-stream approximations. *Beitr. Phys. Atmos.*, **67**, 195–199.

——, and J. A. Davies, 1989a: Surface albedo estimates from *Nimbus-7* ERB data and a two-stream approximation of the radiative transfer equation. *J. Climate*, **2**, 409–419.

——, and ——, 1989b: Comparison between measured and modelled cloudless-sky irradiances at the surface and at the top of the atmosphere. *Atmos.–Ocean*, **27**, 716–727.

——, and ——, 1992: Cumulus cloud radiative properties and the characteristics of satellite radiance wavenumber spectra. *Remote Sens. Environ.*, **42**, 51–64.

——, Z. Li, and J.-P. Blanchet, 1994: Radiative characteristics of the Canadian Climate Centre, second-generation general circulation model. *J. Climate*, **7**, 1070–1091.

Berger, A., and M. F. Loutre, 1993: Precession, eccentricity, obliquity, insolation, and paleoclimates. *Long Term Climatic Variations, Data and Modelling*, J.-C. Duplessy, Ed., NATO ASI, 1–45.

Cahalan, R. F., W. Ridgway, W. J. Wiscombe, T. L. Bell, and J. B. Snider, 1994: The albedo of fractal stratocumulus clouds. *J. Atmos. Sci.*, **51**, 2434–2455.

Cess, R. D., and I. L. Vulis, 1989: Inferring surface solar absorption from broadband satellite measurements. *J. Climate*, **2**, 974–996.

Coakley, J. A., Jr., and P. Chýlek, 1975: The two-stream approximation in radiative transfer: Including the angle of the incident radiation. *J. Atmos. Sci.*, **32**, 409–418.

——, and R. D. Cess, 1985: Response of the NCAR Community Climate Model to the radiative forcing of the naturally occurring tropospheric aerosol. *J. Atmos. Sci.*, **42**, 1677–1692.

Cox, C., and W. Munk, 1956: Slopes of the sea surface deduced from photographs of the sun glitter. *Bull. Scripps Inst. Oceanog.*, **6**, 401–488.

Fouquart, Y., B. Bonnel, and V. Ramaswamy, 1991: Intercomparing shortwave radiation codes for climate models. *J. Geophys. Res.*, **96**, 8955–8968.

Garratt, J. R., 1994: Incoming shortwave fluxes at the surface—a comparison of GCM results with observations. *J. Climate*, **7**, 72–80.

Gates, W. L., 1992: The Atmospheric Model Intercomparison Project. *Bull. Amer. Meteor. Soc.*, **73**, 1962–1970.

Gauthier, C., G. Diak, and S. Masse, 1980: A simple physical model to estimate incident solar radiation at the surface from GOES satellite data. *J. Appl. Meteor.*, **19**, 1005–1012.

Hansen, J. E., D. Russell, D. Rind, P. Stone, A. Lacis, L. Travis, S. Lebedeff, and R. Ruedy, 1983: Efficient three-dimensional global models for climate studies: Models I and II. *Mon. Wea. Rev.*, **111**, 609–662.

Henyey, L. C., and J. L. Greenstein, 1941: Diffuse radiation in the galaxy. *Astrophys. J.*, **93**, 70–83.

Jonas, P. R., R. J. Charlson, and H. Rodhe, 1995: Aerosols. *IPCC 94: Climate Change 1994*, Cambridge University Press, 127–162.

Kiehl, J. T., and B. P. Breigleb, 1993: The relative role of sulfate aerosols and greenhouse gases in climate forcing. *Science*, **260**, 311–314.

Li, Z., and H. G. Leighton, 1993: Global climatologies for solar radiation budgets at the surface and in the atmosphere from 5 years of ERBE data. *J. Geophys. Res.*, **98**, 4919–4930.

——, and L. Garand, 1994: Estimation of surface albedo from space: A parameterization for global application. *J. Geophys. Res.*, **99**, 8335–8350.

——, and H. W. Barker, 1994: Solar energy disposition: Intercomparison between satellite estimation, GCM simulation, and surface observations. *WCRP-IAMAS Int. Workshop on Clouds-Radiation-Climate Interactions and Their Parameterization in Models*. Camp Springs, MD, World Meteor. Org., 110–113.

——, H. G. Leighton, K. Masuda, and T. Takashima, 1993a: Estimation of SW flux absorbed at the surface from TOA reflected flux. *J. Climate*, **6**, 317–330.

——, ——, and R. D. Cess, 1993b: Surface net solar radiation estimated from satellite measurements: Comparisons with tower observations. *J. Climate*, **6**, 1764–1772.

——, C. H. Whitlock, and T. P. Charlock, 1995a: Assessment of the global monthly mean surface insolation estimated from satellite measurements using global energy balance archive data. *J. Climate*, **8**, 315–325.

——, H. W. Barker, and L. Moreau, 1995b: The impact of clouds on absorption of solar radiation by the atmosphere. *Nature* **376**, 486–490.

McClatchey, R. A., R. W. Fenn, J. E. A. Selby, F. E. Volz, and J. S. Garing, 1972: Optical properties of the atmosphere, 3d ed., AFCRL-72-0497, 108 pp. [NTIS N7318412.]

McFarlane, N. A., G. J. Boer, J.-P. Blanchet, and M. Lazare, 1992: The Canadian Climate Centre second-generation general circulation model and its equilibrium climate. *J. Climate*, **7**, 1013–1044.

Payne, R. E., 1972: Albedo of the sea surface. *J. Atmos. Sci.*, **29**, 959–970.

Pinker, R. T., and J. A. Ewing, 1985: Modeling surface solar radiation: Model formulation and validation. *J. Climate Appl. Meteor.*, **24**, 389–401.

Ramaswamy, V., and S. M. Freidenreich, 1992: A study of broadband parameterizations of the solar radiative interactions with water vapor and water drops. *J. Geophys. Res.*, **97**, 11 487–11 512.

Rothman, L. S., 1981: AFGL atmospheric absorption line parameters compilation: 1980 version. *Appl. Opt.*, **20**, 791–795.

Slingo, A., and J. M. Slingo, 1991: Response of the National Center for Atmospheric Research community climate model to improvements in the representation of clouds. *J. Geophys. Res.*, **96**, 15 341–15 357.

Tanre, D., J.-F. Geleyn, and J. Slingo, 1984: First results of the introduction of an advanced aerosol-radiation interaction in the ECMWF low resolution global model. *Aerosols and Their Climatic Effects*, H. E. Gerber and A. Deepak, Eds., Deepak Publishing, 133–177.

Thekaekara, M. P., 1974: Extraterrestrial solar spectrum, 3000–6100 Å at 1-Å intervals. *Appl. Opt.*, **13**, 518–522.

Wiscombe, W. J., and G. W. Grams, 1976: The backscattered fraction in two-stream approximations. *J. Atmos. Sci.*, **33**, 2440–2451.